Wave slope and wave age effects in measurements of electromagnetic bias

W. Kendall Melville, Francis C. Felizardo,[1] and Peter Matusov

Scripps Institution of Oceanography, University of California, San Diego, La Jolla, California, USA

Received 10 November 2002; revised 30 November 2003; accepted 20 January 2004; published 27 July 2004.

[1] We present measurements of Ku band electromagnetic (EM) bias made for 2 months from a platform in Bass Strait off the southeast coast of Australia during the austral winter of 1992. EM bias, ϵ, the difference between the electromagnetic and true mean sea levels, was measured using Doppler scatterometers. Linear wave theory was used to relate the Doppler signal to the surface displacement, giving simultaneous coincident backscatter and wave measurements, including significant wave height, H_s. On the basis of dimensional reasoning, we suggest that the usual inhomogeneous correlations of the normalized bias $\beta = \epsilon/H_s$ with the 10 m wind speed, U_{10}, and H_s may be improved by correlating the data with nondimensional variables, including a characteristic wave slope, s, and wave age, c/U_{10}, where c is a characteristic phase speed of the surface waves. Using both polynomial correlations and optimal estimation techniques to fit the data, we find that the standard error of the fit is reduced by $\sim$50% when the dimensionless variables are used. We find that the dependence of the EM bias on the wave slope is consistent with earlier tower-based measurements and the theory of short-wave modulation by longer waves. We discuss the implications of these results for operational implementation of EM bias algorithms based on wave slope and wave age. *INDEX TERMS:* 4275 Oceanography: General: Remote sensing and electromagnetic processes (0689); 4594 Oceanography: Physical: Instruments and techniques; 6969 Radio Science: Remote sensing; *KEYWORDS:* EM bias, radar altimetry, remote sensing

Citation: Melville, W. K., F. C. Felizardo, and P. Matusov (2004), Wave slope and wave age effects in measurements of electromagnetic bias, *J. Geophys. Res.*, *109*, C07018, doi:10.1029/2002JC001708.

1. Introduction

[2] Electromagnetic (EM) bias remains one of the largest errors in radar altimetry for oceanographic applications. It results from the fact that, on average, the troughs of the surface waves are better reflectors of radio waves than are the crests, resulting in the electromagnetic mean sea level being lower than the true mean sea level. This difference is known as the EM bias. It was first discovered in tower-based measurements by *Yaplee et al.* [1971], and subsequent tower [*Melville et al.*, 1991; *Arnold et al.*, 1995] and aircraft [*Walsh et al.*, 1991; *Hevizi et al.*, 1993] measurements have confirmed the effect and correlated the bias, ϵ, with the wind speed, U_{10}, and significant wave height, H_s. Attempts have also been made to infer the EM bias from the altimeter data itself, by making certain hypotheses about the variability of the ocean between overflights [*Chelton*, 1994; *Gaspar et al.*, 1994]. In general, the aircraft and space-based results have led to estimates of the normalized bias, $\beta = \epsilon/H_s$, that are less than the tower-based measurements; however, *Gaspar and Florens* [1998] have recently revised their earlier nonparametric estimates of the bias, to give improved agreement with the tower-based measurements.

[3] A fundamental criticism of earlier attempts to correlate EM bias with wind and wave variables is that the resulting relationships have been inhomogeneous, giving the dimensionless bias, β, in terms of the dimensional significant wave height, H_s, and the dimensional wind speed, U_{10}. The pragmatic reason for the use of these correlations is that both the wave height and the wind speed can be inferred from the altimeter measurements, and if accurate, the correlations would make the altimeter a "self-contained" instrument, not dependent on external measurements for EM bias corrections. However, as new uses of altimetry demand greater accuracy, it may be that this outweighs the convenience of a self-contained system for EM bias, and supplementary measurements become necessary.

[4] It is instructive to consider the problem in the context of simple dimensional analysis. Let us assume that the EM bias, ϵ, is dependent on the small-scale roughness of the ocean surface, which is mainly a function of both the wind speed, U_{10}, (as is assumed in scatterometry) and the structure of the ocean surface at the scale of the longer wind waves and swell. The small-scale roughness may be modulated by the longer waves, or the direct nonlinear effects of the longer wind waves may be significant. In either case, we assume that the longer surface waves can be

[1] Now at Union Cement Corporation, Makati City, Philippines.

0148-0227/04/2002JC001708

represented by a characteristic amplitude, $a_l = H_s/2$, say, and a characteristic wave number, k_l, and radian frequency, ω_l. In mixed wind seas and swell, the slope of the swell is usually significantly less than that of the wind waves. The EM bias is also a function of the wave number of the radio waves, k_r, but to include this effect the details of the small-scale roughness must also be represented [*Arnold*, 1992], and its representation by just U_{10} is inadequate. So, we limit ourselves to considering the functional relationship for just one radio wavelength. Thus we have that

$$\epsilon = \epsilon(H_s, U_{10}, k_l, \omega_l, \ldots). \quad (1)$$

Now, by dimensional reasoning it follows that

$$\beta = \beta(H_s k, U_{10} k/\omega_l, \ldots) \quad (2)$$

or

$$\beta = \beta(a_l k_l, U_{10}/c_l, \ldots), \quad (3)$$

where $a_l k_l$ is a measure of the slope of the longer waves and U_{10}/c_l is the reciprocal of the wave age. One of the primary aims of this paper then is to determine whether a dimensionally homogeneous correlation of the dimensionless bias with the wave slope and wave age gives an improvement over the dimensionally inhomogeneous, but pragmatic correlations that have been used in the past.

[5] The structure of the paper is as follows. In section 2 we describe the experimental site and the essential details of the measurements. In section 3 we present the techniques of data analysis and technical details of some of the measurements and calibrations, including the technique used to estimate a characteristic slope of the surface waves based on the linear dispersion relationship and the measurements of wave height. In section 4 we present the measurements of EM bias over the course of the experiment, and show the usual correlations of EM bias with wind speed and wave height. We also show the improved correlations of normalized EM bias with the wave slope and wave age, and present both polynomial fits and optimized empirical fits to the data. In section 5 we review the major results of the paper and discuss the implications of these results for operational EM bias corrections.

[6] Preliminary versions of this work have been presented as posters at the TOPEX/Poseidon Jason-1 Science Working Team Meetings in 1998 and 1999 and at the Air-Sea Interface Symposium (Sydney, Australia) in 1999; they have also been posted on our Web site (http://airsea.sio.ucsd.edu). The data presented here have subsequently been used in several studies that also address the use of wave slope in describing EM bias using the data described here. *Millet et al.* [2003a, 2003b], using this Bass Strait data supplemented by earlier tower data from the Gulf of Mexico [*Arnold et al.*, 1995], show that the extended data set confirms the basic result of *Melville et al.* [1999] (see http://airsea.sio.ucsd.edu/Posters/EMBposter.pdf) that the rms error in estimating bias is reduced by ~50% when using wave slope instead of the usual parameterizations by wind speed and wave height. *Millet et al.* [2003a, 2003b] analyzed the two tower data sets and TOPEX/Poseidon data showing improved correlations between models of bias based on the in situ data and the satellite data. *Gommenginger et al.* [2003], using wave model (WAM) wave computations, show that the *Srokosz* [1986] model of sea-state bias leads to a quasi-linear relationship between the sea-state bias coefficient and the r.m.s. slope of the longer gravity waves, and shows good agreement with the tower data of *Melville et al.* [1991] and the data reported here. They also found that the EM bias predictions of the theory of *Elfouhaily et al.* [2000] were sensitive to the high-frequency tail of the surface wave field. Most recently, *Kumar et al.* [2003] using an EM bias algorithm inferred by the results presented here and the current operational EM bias correction applied to TOPEX/Poseidon data, along with buoy measurements of wind speed and wave spectra and WAM wave modelling, conclude that EM bias corrections cannot be reliably estimated from altimeter data alone, and will require input from coupled ocean-atmosphere models, wave models and perhaps other satellite sensors.

2. Experiment Description

[7] An experiment to study the characteristics of electromagnetic bias was conducted from 16 June to 26 September 1992 (year day 167–325) on the Esso/BHP Snapper platform in Bass Strait, Australia. Two Ku band (14 GHz) coherent, continuous wave, dual-polarized scatterometers built at the US Naval Research Laboratory (Washington, DC) were mounted at two different elevations at the southwest corner of the platform, which is in water 57 m deep, 30 km offshore. Figure 1 shows a map of the location of the experiment off the coast of southeastern Australia.

[8] Figure 2 shows schematic diagrams of the platform and the location of the different instruments, with the scatterometers (K15,K25) mounted 15 and 25 m, respectively, above the mean sea surface. When pointing at nadir the footprints of the scatterometers at the sea surface were at least 8 m away from the main legs of the platform, and in unimpeded wind and wave fields from the southwest half-plane. (It is well known that in storms the region immediately around a platform may be foam covered due to wave/current/platform interaction. We have no relevant observations of these effects for the Snapper platform and no account of foam coverage was taken in editing the data.) Both scatterometers were oriented toward nadir at the start of the experiment. The two-way half-power beam width of both scatterometers is 6.3°, giving 3 dB spot sizes at the sea surface of ~1.7 and 2.7 m diameter for K15 and K25, respectively. The lower scatterometer was reoriented to a 45° incidence angle on 19 August (year day 231) for a different study. We only present the measurements taken prior to that date.

[9] The scatterometers were designed to generate a complex valued output from the horizontally polarized (HH) and vertically polarized (VV) signals. The real and imaginary components of the output were sampled at 3125 Hz by a 12 bit analog-digital (A-D) converter mounted in a personal computer. A separate A-D converter in the same computer was used to simultaneously sample, at 16 Hz, the data from three wire wave gauges and the anemometers. The other meteorological instruments were polled every 10 min. After the initial setup, the experiment ran independently until

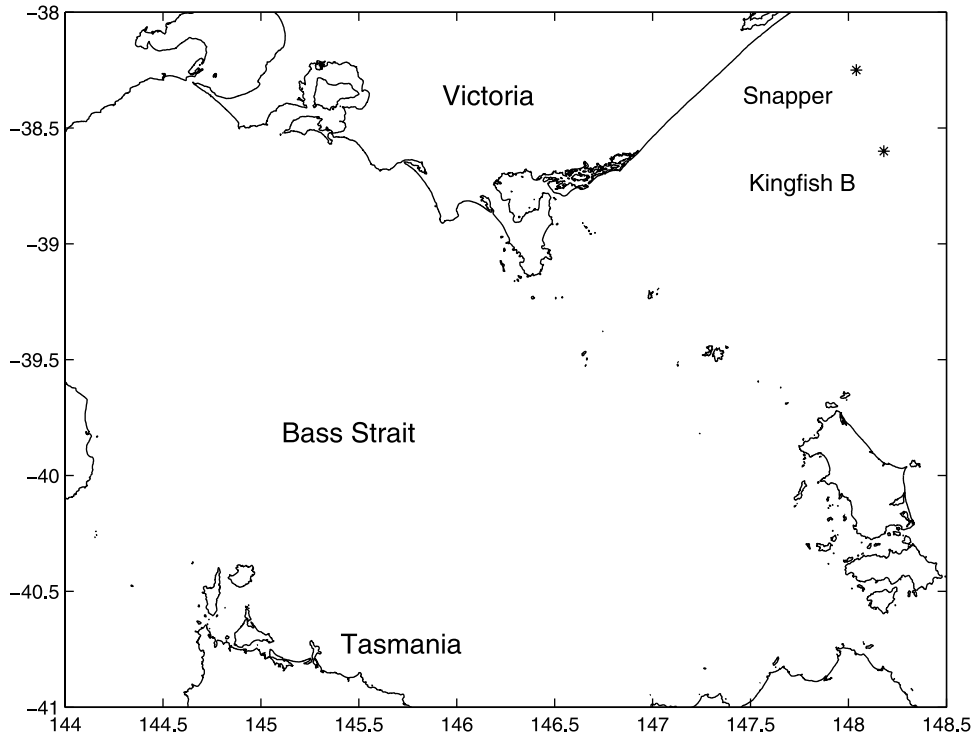

Figure 1. Location of the Esso/BHP Snapper and Kingfish B platforms in Bass Strait. The primary measurements were from Snapper, with some supporting meteorological measurements from Kingfish B.

Julian day 231, with the crew of the platform replacing the optical storage disks every week.

[10] Wind speed and direction measurements were made at a 35 m elevation on the Snapper platform. Similar measurements were made at a 53 m elevation on Kingfish B, a platform 45 km southeast of Snapper. The wind direction sensor of the anemometer at the Snapper platform stopped working on 7 July (Julian day 188). Intercomparison of the anemometer data between the Snapper and Kingfish B platforms prior to that date showed that for winds coming from the southwest half-plane (135°–315°; see below) there was generally excellent agreement between

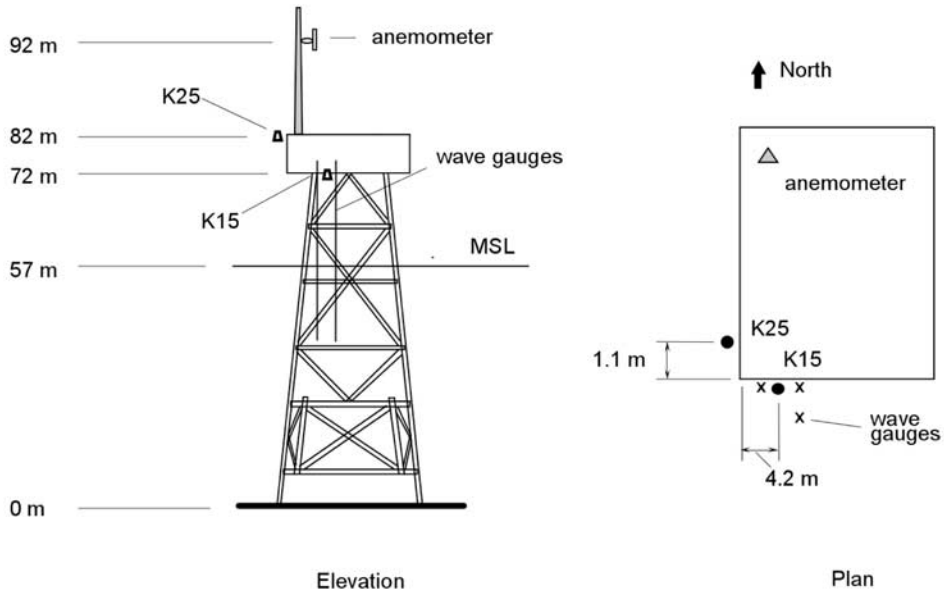

Figure 2. Snapper platform and the location of the primary instruments. K15 and K25 are Ku band Doppler scatterometers at 15 and 25 m above mean sea level (MSL), respectively. The wire wave gauges were separated by 1 m in orthogonal directions. The R. M. Young propeller anemometer was mounted 35 m above MSL.

the wind directions at the two platforms which in a worst case differed by at most 30°. Wind speeds from the same directions were typically within ±1 m/s. This agreement is attributed primarily to the fact that winds in these directions were either from the open sea at fetches much larger than the distance between the platforms or off a broad flat coastal plain. The wind direction data after 7 July were taken from the anemometer on the Kingfish B platform. The wind speed measurements were later reduced to the equivalent wind speed at 10 m elevation, U_{10}, using an assumed logarithmic wind speed profile [*Wu*, 1980; *Smith*, 1988]:

$$U_z \equiv U(z) = \frac{u_*}{\kappa} \ln \frac{z}{z_0}, \tag{4}$$

with the roughness length, z_0, given by

$$z_0 = z_s + z_c = 0.11\nu/u_* + 0.0185u_*^2/g, \tag{5}$$

where $\kappa = 0.4$ is the von Karman constant, u_* the friction velocity, ν the kinematic viscosity of air, and g the gravitational acceleration. Thus we have two equations for the two unknowns u^* and z_0.

[11] Although instruments for measuring air temperature, sea temperature and relative humidity were deployed at the start of the experiment, the sea surface temperature and relative humidity instruments stopped operating after a short period of time. Hence we were unable to incorporate the effects of atmospheric stability in computing the value for U_{10}. *Large and Pond*'s [1981] results suggest that neglecting atmospheric stability will lead to an error of less than 4% in U_{10}.

[12] Three nichrome resistance wire wave gauges were installed on the platform in a triangular pattern near the scatterometer at the 15 m level (K15). The wires were ~1 m apart along the orthogonal sides of the triangle and were calibrated at the beginning of the experiment. This was accomplished by positioning the wires at various predetermined elevations and sampling the mean voltage over several minutes at each position. On 19 August (Julian day 231), the wires were again calibrated, cleaned and calibrated again.

3. Data Editing and Processing

3.1. Overview

[13] Figure 3 shows time series of the 10 m wind speed, U_{10}, and direction, θ_w, (direction from which the wind is coming), the significant wave height, H_s, (from the K15 Doppler scatterometer measurements; see below), and the phase speed c at the peak of the wind wave spectrum, during the 64 day observation period. The measured hourly averaged values of U_{10} range from 0.6 to 15.4 m/s. Wind speeds up to 20 m/s were observed, although these events did not last more than 20 min.

[14] Since the scatterometers and wave gauges were positioned near the southwest corner of the platform, wind and waves coming from directions close to azimuth $\theta_w = 225°$ are subjected to the least interference from the platform. The limits of the half-plane of θ_w values within $225° \pm 90°$ are denoted in Figure 3b by the two dashed lines. Of the 1539 available hourly averages, 814 (53%) are included within this half-plane, for which the minimum fetch is 50 km to the northwest, extending to ~500 km to the southwest and essentially infinite fetch to the southeast.

[15] The determination of the peak of the wind wave spectrum is relatively unambiguous in a multimodal spectrum but in unimodal spectra it is less clear. In analyzing these data we have set c equal to the phase speed at the peak of unimodal spectra. In consequence of this, we expect to be measuring the phase speed of the swell at low wind speeds. The data in Figure 3d show that the largest phase speeds were ~15 m/s, corresponding to a wavelength of ~145 m. In a water depth of 57 m, the correction to the phase speed for finite depth effects is less than 1% for waves of this length. Thus we expect the kinematics of the wave field to correspond to deep water conditions.

3.2. Scatterometers

[16] The scatterometer output time series were processed in the time domain using the covariance processing technique [*Doviak and Zrnic*, 1984]. Our implementation of this method follows closely the method described and used by *Jessup et al.* [1991], which gives a direct estimate of the power, mean frequency and bandwidth of the complex valued time series for each polarization (HH, VV) every 0.0625 s. They were then saved to optical disks every 10 min together with the meteorological data and the wire wave gauge data. Hourly averages of the time series were later computed and used in this study.

[17] The scatterometers were calibrated immediately before and after deployment by measuring the rms amplitude of the complex valued output voltage of each polarization of the scatterometer using a 15 cm aluminum sphere as a target. The procedure used is described in detail by *Jessup* [1990]. The results show that the drift in the calibration of both channels of the K25 scatterometer was minimal. The same is true with the HH channel of K15 although the drift was slightly larger in this case. The calibration of the K15 VV channel on the other hand differed significantly before and after the experiment due to damage to one of the wave guides. An inspection of the hourly averaged time series of the cross section, σ_0, showed that this occurred on approximately day 200, 32 days after the start of the experiment. While adjusting the calibration factors for the VV channel to account for this would have been feasible, we decided to avoid using potentially unreliable K15 VV data after that date.

[18] In computing σ_0, we note that the value of the normalized scatterometer varies with the target range R and the illuminated area A. Since the presence of surface waves modifies the range to the sea surface, a correction to the value of the measured cross section $\sigma_{0,\mathrm{meas}}$ needs to be applied. The value of σ_0 is proportional to R^{-4} and to A. On the other hand, the illuminated area A is proportional to R^2. Hence the net value of σ_0 varies as R^{-2}. The scatterometer cross section σ_0 is related to the measured scatterometer cross section $\sigma_{0,\mathrm{meas}}$ by

$$\sigma_0 = K \frac{(H-\eta)^2}{H^2} \sigma_{0,\mathrm{meas}}, \tag{6}$$

where K is a calibration factor, H is the height of the scatterometer above the mean sea level and η is the sea

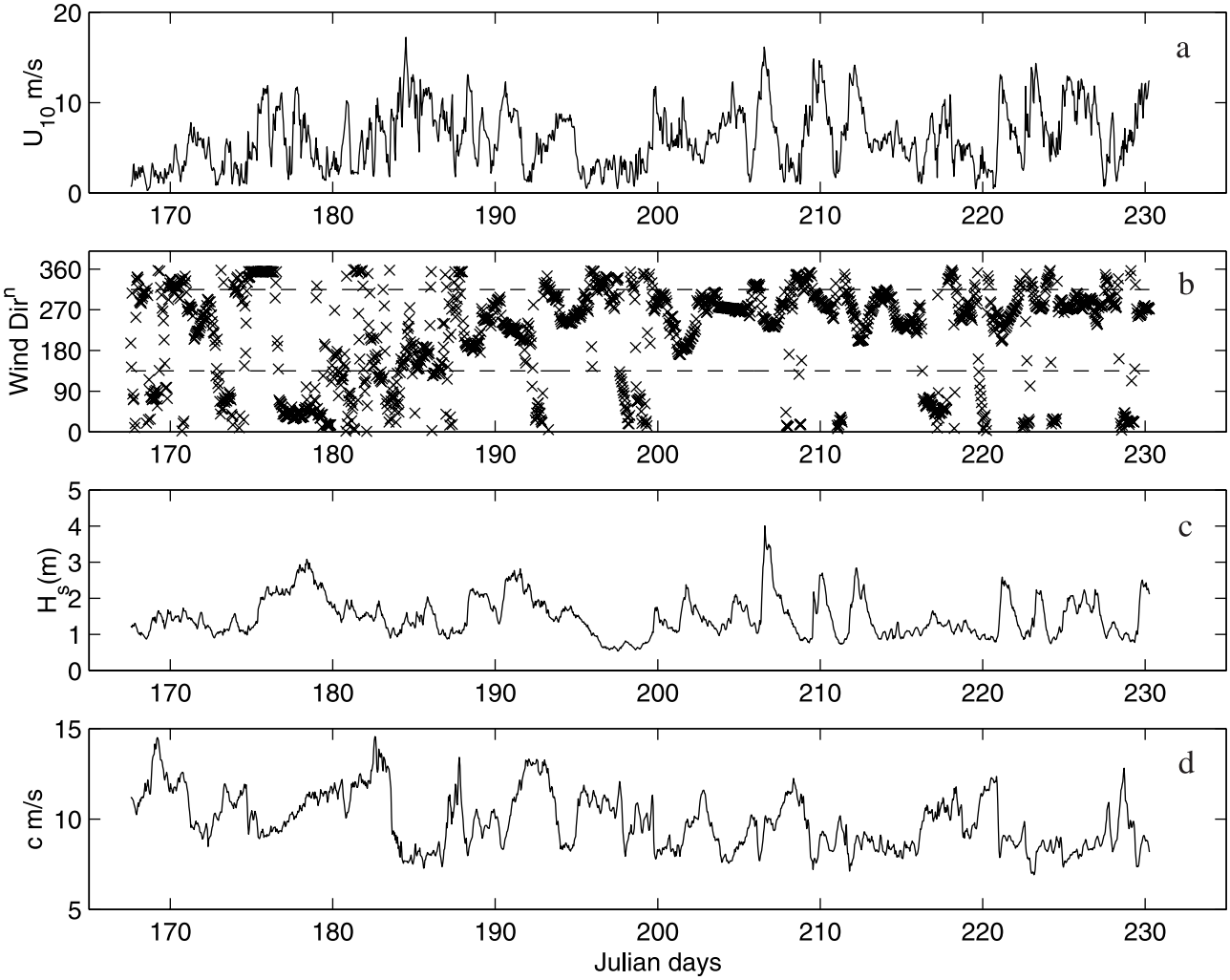

Figure 3. Time series of hourly averages of (a) the 10 m wind speed, U_{10}, (b) the direction from which the wind was coming, θ_w, (c) the significant wave height, H_s, and (d) the phase speed at the peak of the (wind wave) spectrum (see text) for the duration of the experiment. The dashed lines at 135° and 315° in Figure 2b show the limits of the wind direction sector that was used to avoid interference from the platform. Only data in this sector contributes to the final results in this paper.

surface displacement at the scatterometer footprint as measured by the scatterometer (see below).

3.3. Doppler Wave Gauge

[19] Since the wire wave gauges were located outside the footprint of the two scatterometers, parameters such as EM bias which require sea surface measurements that are coincident with the scatterometer footprint cannot be computed from wire wave gauge data. We instead use the measured Doppler shift from both scatterometers to infer the fluctuation of the sea surface elevation at the footprint of both scatterometers. This method was earlier used by *Arnold et al.* [1995] and the errors are reviewed here.

[20] The kinematics of the sea surface are described by the free surface boundary condition

$$\frac{d\eta}{dt} = \frac{\partial \eta}{\partial t} + u\frac{\partial \eta}{\partial x} + v\frac{\partial \eta}{\partial y} = w, \tag{7}$$

where $\mathbf{u} = (u, v, w)$ is the velocity of the water at the surface $z = \eta$. For slowly varying waves of small slope, i.e., $a_l k_l \ll 1$, to leading order, the advective terms may be neglected, introducing an error of the order of $(a_l k_l)$:

$$w = \frac{\partial \eta}{\partial t}[1 + O(a_l k_l)]. \tag{8}$$

The sea surface slopes over scales comparable to the footprint of the scatterometers are typically in the range $O(10^{-2}–10^{-1})$.

[21] An additional correction is required since the scatterometer measures the Doppler shift due to the motion of the scatterers within the footprint. It is easy to show that this leads to an error of $O(c_s/c_l)$, where c_s is the intrinsic phase speed of the (unresolved) scatterers and c_l is the phase speed of the longer (resolved) waves. We expect that for typical conditions $c_s/c_l \ll 1$. The time series of the surface elevation can then be well approximated by integrating the vertical velocity, w, with respect to time.

[22] The ability of this technique to resolve high-frequency waves is limited by the size of the illuminated area, so

that K15, which has a smaller footprint than K25, will be able to resolve the smaller waves better than K25. We can estimate the maximum frequency resolution of the two scatterometers using the deep water dispersion relation

$$\omega^2 \equiv (2\pi f)^2 = gk. \tag{9}$$

[23] The scatterometer can not resolve surface wave lengths equal to or shorter than the diameter L of the illuminated area A. Using this assumption and equation (9), the limit on the maximum surface wave frequency the method can resolve is

$$f_m \approx \sqrt{\frac{g}{2\pi L}}. \tag{10}$$

[24] For K15, $f_m \approx 0.9$ Hz and for K25, $f_m \approx 0.7$ Hz. Figure 3c shows the significant wave height H_s deduced from the K15 HH Doppler frequency. H_s measured using the other scatterometer is virtually indistinguishable from this time series. The value of H_s ranges from 0.6 to 4.8 m. Owing to the presence of swell, H_s is nonzero even in the absence of wind.

3.4. Wave Gauge Comparisons

3.4.1. Wave Height

[25] Figure 4a compares the time series of the sea surface elevation η derived from K15, K25 and wire wave gauge C. The data were taken 3 days after the initial calibration under low wind speeds ($U_{10} \approx 2.4$ m/s). The sea surface fluctuations are dominated by swell with $H_s = 1.5$ m. These values are typical of the conditions during the first week of the experiment. The three instruments are measuring the sea surface elevation at three slightly different horizontal locations (see Figure 2), but show good agreement between the Doppler scatterometers and the wire wave gauge.

[26] In general, the two methods give time series that are comparable except at the crest and troughs of the steepest waves. At these locations, the wire wave gauge gives larger values of the wave height than the scatterometers. The discrepancies in the wave height measured by the two methods are due to errors associated with neglecting higher-order slope terms, terms of $O(c_s/c_l)$, and the finite size of the scatterometer footprints.

[27] The effects of the differences in the footprint size are apparent in Figure 4b, which shows typical wave height frequency spectra $\Phi(f)$ derived from K25, K15 and wire wave gauge C. The spectra were computed from $\sim$1 hour of data and show that while the spectral levels at the energy-containing portion of both scatterometer spectra are nearly equal, the K25 spectral level falls off at a steeper slope than that of K15. This shows that of the two scatterometers, K15 is better able to resolve the high-frequency characteristics of the surface wave spectrum.

[28] Figure 4b also shows that the spectral level of wire wave gauge C at frequencies larger than $\sim$0.5 Hz is greater than that for the scatterometer derived spectra, with the difference increasing at the higher frequencies. As mentioned earlier, the scatterometer Doppler resolution is limited to waves larger than the size of the footprint which is in the range of 1–3 m. In contrast, the wire wave gauge measurement area is comparable to the wire diameter: a few millimeters. Hence the wire wave gauge is able to resolve higher surface wave frequencies much better than either scatterometer. An orthogonal regression [*Casella*, 1990, p. 584] of H_s measured by K15 and K25 gives

$$H_{s(\mathrm{K15})} = 1.04 H_{s(\mathrm{K25})} - 0.017 \tag{11}$$

in meters. That is, the difference in the elevation, and consequently the spot size, of the two scatterometers leads to a 4% discrepancy in the H_s estimates.

3.4.2. Wave Slope

[29] The effect of the difference in the illuminated area, and consequently the ability of the scatterometers to resolve higher-frequency waves, is seen more readily when the wave slope spectrum $S(f)$ is deduced from $\Phi(f)$, the surface displacement spectrum. A measure of the rms wave slope s can be computed from Φ and the linear dispersion relationship using the relations [*Cox and Munk*, 1956]

$$S(f_i) = \frac{(2\pi f_i)^4}{g^2}\Phi(f_i) \tag{12}$$

$$s = \left[\frac{1}{N}\sum_{i=1}^{N}\frac{(2\pi f_i)^4}{g^2}\Phi(f_i)\right]^{1/2}. \tag{13}$$

Figure 4c shows plots of the wave slope spectra $S(f)$ from K25 and K15 and wire wave gauge C computed using equation (12) and the wave height spectra $\Phi(f)$ in Figure 4b. As expected, the differences in the spectral levels of $S(f)$ between the two scatterometers are more pronounced at the higher frequencies. We can also see that compared to $\Phi(f)$, the spectral level at the higher frequencies of $S(f)$ has a more significant effect on the value of s. The accurate determination of the full rms wave slope s, is fraught with difficulties associated with an appropriate choice of the cutoff frequency, and with the use of the linear dispersion relationship [*Felizardo and Melville*, 1995]. Recent work [*Fedorov et al.*, 1998] suggests that the cutoff frequency required to give the full rms wave slope may be as high as $O(100)$ Hz. However, we are only concerned with estimating the contribution to the rms slope from waves comparable in scale or longer than the diameter of the footprint of the scatterometer, s_l, say. For these purposes, we can use the cutoff of K15 at $\sim$1 Hz (see Figure 4b), which leads to larger estimates of s_l from K15 than from K25 as shown in Figure 5a. Linear regression of the data gives

$$s_{l\mathrm{K15}} = 1.12 s_{l\mathrm{K25}} + 0.005. \tag{14}$$

[30] Since the difference between s_l computed using the two scatterometers can be significant, we will be using $s_{l\mathrm{K15}}$ as the value of s_l in subsequent figures. However, Figure 4 suggests that estimates of s_l based on K15 may still slightly underestimate the rms slope of the longer waves.

3.5. Wave Age

[31] Wave age, the ratio of a characteristic surface wave phase speed to the wind speed, c/U_{10}, is a measure of the strength of the wind forcing and wave growth. For low

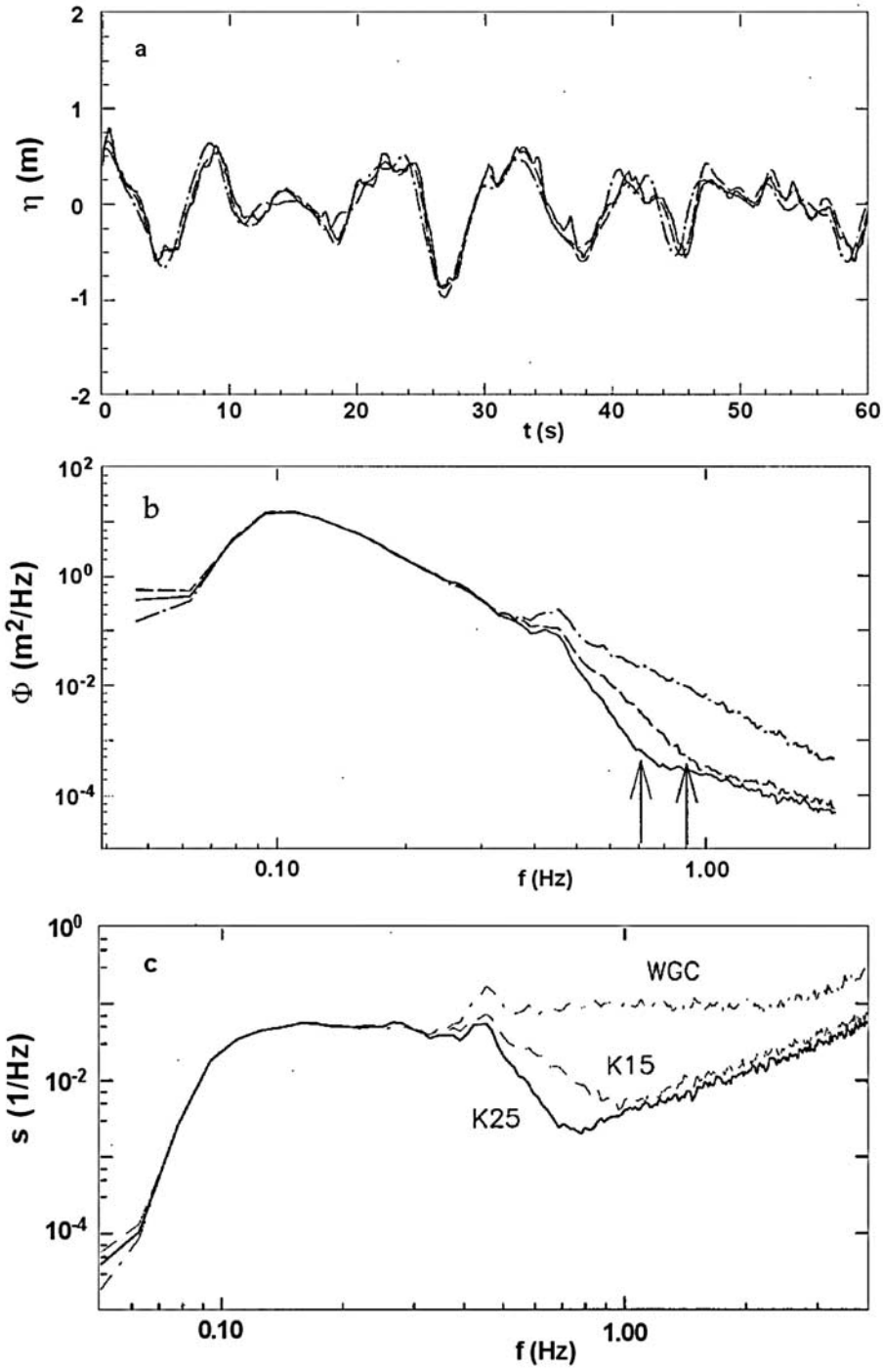

Figure 4. Intercomparisons of (a) surface displacement measurements, (b) wave amplitude spectra, and (c) slope spectra from K15 (dashed lines), K25 (solid lines), and a wire wave gauge (dash-dotted lines) on Julian day 170. Note that the separation of the instruments by horizontal distances of $O(1)$ m account for some of the differences in Figure 3a but should have no effect on the spectra. The arrows in Figure 3b denote the cutoff frequencies of 0.9 Hz and 0.7 Hz based on the footprints of K15 and K25, respectively. The small local peaks in the spectra at 0.4–0.5 Hz are most likely due to interference from the leg of the platform. The ''slope'' spectrum is based on the wave spectrum and the linear dispersion relationship for deep water waves and is only an approximation to the true slope spectrum.

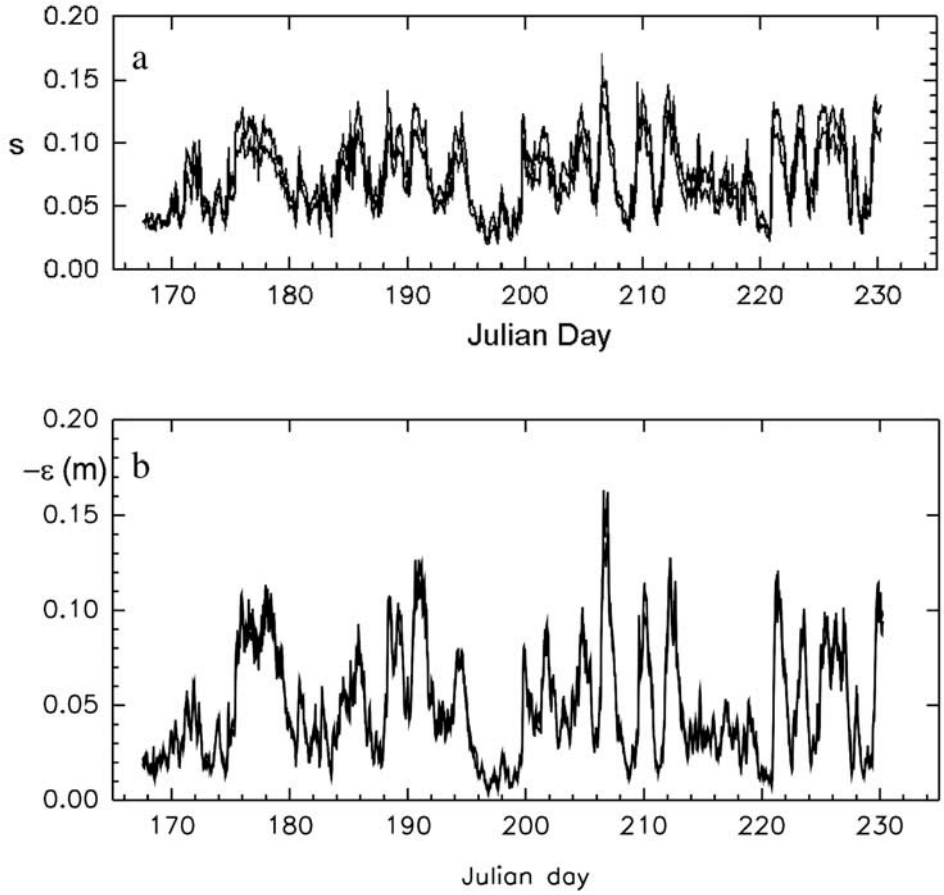

Figure 5. (a) Hourly time series of rms slope, s, computed using K15 (solid line) and K25 (dashed line). Over the course of the experiment we found that due to the larger footprint, K25 gave values of s ~12% less than K15. The K15 values were subsequently used in the analysis of the data. (b) Hourly time series of EM bias measured by K15 (solid line) and K25 (dashed line). Note the obvious visual correspondence between events of large s and large magnitude of ϵ and the fact that the two time series are almost indistinguishable, except at the larger values of bias.

values of c/U_{10}, the waves are strongly forced and growth rates, normalized by the wave frequency corresponding to c, are high. For values of wave age around unity the growth rates are very small and may change sign as unity is exceeded [*Komen et al.*, 1994].

[32] The wave age is not unique for a given set of conditions as it depends on the choice of c from a spectrum of surface waves. In our case we choose c to represent waves at the peak of the wind sea spectrum, f_p, so $c_p \equiv c(f_p)$. The wave height spectrum may have peaks representing both wind waves and swell, but the contribution of the swell to the wave slope is generally much less than that of the local wind-generated waves. Furthermore, in a preliminary analysis using coherence techniques to study the frequencies contributing most to the correlation between the surface displacement and backscattered power, the source of EM bias, we found the coherence to be significant only at frequencies greater than the peak of the wind wave spectrum.

[33] In the absence of directional wave measurements, we simply used the presence of multiple peaks in the spectrum to distinguish between wind seas and swell for the purposes of defining c_p. For unimodal spectra, we used the single peak to define c_p.

3.6. Electromagnetic Bias

[34] The EM bias ϵ is a shift in the mean reflecting surface measured by the altimeter due to the greater reflectivity of the wave troughs than the wave crests. Its value is computed from measurements of the scatterometer cross section σ_0 and the sea surface elevation η with

$$\epsilon = \frac{\sum_{n=1}^{N} \sigma_0(t_n)\eta(t_n)}{\sum_{n=1}^{N} \sigma_0(t_n)} \tag{15}$$

at the full temporal resolution of the measurements. If σ_0 and η are completely uncorrelated, then ϵ is equal to zero.

4. Results

[35] Over the 2 month deployment of this experiment, the hourly averaged wind speed U_{10} ranged from 0.6 to 15.4 m/s, the significant wave height H_s from 0.7 to 4.0 m,

and the rms wave slope s from 0.02 to 0.16. Linear regressions between the HH and VV data in the calculation of the EM bias showed that K15HH was 6% smaller than K15VV and K25HH was 3% larger than K25VV. These differences remain unexplained and for isotropic distributions of the surface wave field must be considered as measures of instrument error in measuring the EM bias. Figure 5b shows time series of the hourly averaged ϵ measured by the HH channels of the K15 and K25 scatterometers. These data are almost indistinguishable except at the largest biases. Note that ϵ is always negative and ranged from -0.005 to -0.16 m during the course of the experiment.

4.1. EM Bias, Wave Height, and Wind Speed

[36] Figure 6 shows plots of the measured binned normalized bias β, for K15 and K25, as a function of U_{10}, with the residual binned as a function of H_s. Also shown are $\tilde{\beta} = \beta_1(U_{10}) + \beta_2(H_s)$ third-order polynomial fits to β for each elevation. The data are binned in increments of 1 m/s for U_{10} and 0.2 m increments for H_s. This traditional way of displaying the data and the polynomial representation in terms of the wind speed and significant wave height show some of the ambiguity that can result as $\tilde{\beta}$ does not go to zero as both U_{10} and H_s go to zero.

[37] It is instructive to display the data in the (U_{10}, H_s) plane as shown in Figure 7. Here Figure 7a is the measured normalized bias, β_{K15}, plotted in the plane; Figure 7b is the third-order polynomial fit to the data; Figure 7c is the residual, and Figure 7d is the data merged with the polynomial fit. The corresponding figure for K25 (not shown here) is very similar. The polynomial fits for the K15 and K25 data (expressed as a percentage) in the (H_s, U_{10}) plane are

$$\tilde{\beta}_{K15} = -0.12 + 0.312U_{10} + 0.008U_{10}^2 - 0.001U_{10}^3 + 1.418H_s - 0.243H_s^2 - 0.013H_s^3 \quad (16)$$

$$\tilde{\beta}_{K25} = 0.865 + 0.120U_{10} + 0.023U_{10}^2 - 0.001U_{10}^3 + 0.716H_s + 0.059H_s^2 - 0.059H_s^3, \quad (17)$$

with standard deviations of 0.61% and 0.54%, respectively.

4.2. EM Bias, Wave Slope, and Wave Age

4.2.1. Polynomial Fits

[38] In section 1 we argued that a more rational correlation for the normalized bias, β, would be with the wave slope, s_l, and the wave age, or reciprocal wave age, U_{10}/c_l. Figure 8 shows the binned normalized bias data for K15 and K25 plotted against these dimensionless variables, along with third-order polynomial fits to the data. We use the same notation as in Figure 6 with $\tilde{\beta} = \beta_1(s_l) + \beta_2(U_{10}/c_l)$, where β_1 now represents the binned β data and its polynomial fit as a function of s_l, and β_2 represents the residual and its polynomial fit as a function of U_{10}/c_l. Comparison with Figure 6 shows a qualitative and quantitative improvement in the representation of the data using the dimensionless independent variables. Most obvious is the reduction in the scatter of the data when plotted against s_l (c.f. Figures 6a and 8a). Also, the intercept for $\beta_1(s)$ is essentially zero, and the range of the residual signal to be correlated with the wave age, $\beta_2(U_{10}/c)$, is reduced by a factor of 2–3 when compared with that for $\beta_2(H_s)$.

[39] The improved correlations with the dimensionless variables become clear when the data for K15 is plotted in the (s, U_{10}/c) plane as shown in Figure 9a. Also shown is the third-order polynomial fit to the data (Figure 9b), the difference between the data and the polynomial fit (Figure 9c), and the data merged with the polynomial fit (Figure 9d). What is immediately clear is that the dependence of β on s is significantly stronger than that on U_{10}/c; that is, the isolines of β are almost vertical. The corresponding results for K25 (not shown here) are similar. The polynomial fits for K15 and K25 (expressed as a percentage) are

$$\tilde{\beta}_{15} = -0.458 + 36.3s_l + 294s_l^2 - 2331s_l^3 + 0.34\frac{U_{10}}{c_l} + 0.28\left[\frac{U_{10}}{c_l}\right]^2 - 0.17\left[\frac{U_{10}}{c_l}\right]^3, \quad (18)$$

and

$$\tilde{\beta}_{25} = -0.206 + 42.9s_l + 156s_l^2 - 1829s_l^3 - 0.769\frac{U_{10}}{c_l} + 1.264 \cdot \left[\frac{U_{10}}{c_l}\right]^2 - 0.417\left[\frac{U_{10}}{c_l}\right]^3, \quad (19)$$

with standard errors of 0.28% and 0.31%, respectively; ~50% less than those for the (H_s, U_{10}) fits. Examination of the data in Figure 8 shows that the primary contribution to the constants in each polynomial fit comes from the residual associated with the wave age (Figure 8c).

4.2.2. Objective Mapping

[40] *Gaspar and Florens* [1998] have recently drawn attention to the fact that parametric models of the EM bias are not true least squares approximations to the empirical data, and that nonparametric methods can yield improved estimates of the bias. In the context of our measurements, the conclusion is that multivariate polynomial fits of the kind presented above do not minimize the error between the estimate and the measurements, since they are constrained by the assumed functional form. One advantage of the parametric models is that they can be represented by a few parameters, whereas the nonparametric estimates require a look-up table to estimate the bias from the independent variables. However, this is not a significant disadvantage for altimetry. In effect, nonparametric, or optimal estimation (objective mapping) techniques, are a way of smoothly interpolating the measured data to minimize the mean square error between the interpolation and the data.

[41] The method used here is a standard implementation of objective mapping or Gauss-Markov interpolation [*Daley*, 1991] using the MIT/SaGA software package written by K. K. Pankratov (1995, see http://puddle.mit.edu/~glenn/kirill/saga.html). On the basis of an analysis of the data we fitted the empirical correlation of the data to a standard correlation function of the form

$$C(x,y) = e\delta(x,y) + (1-e)\exp\left[-\left(\frac{x}{L_x}\right)^2 - \left(\frac{y}{L_y}\right)^2\right], \quad (20)$$

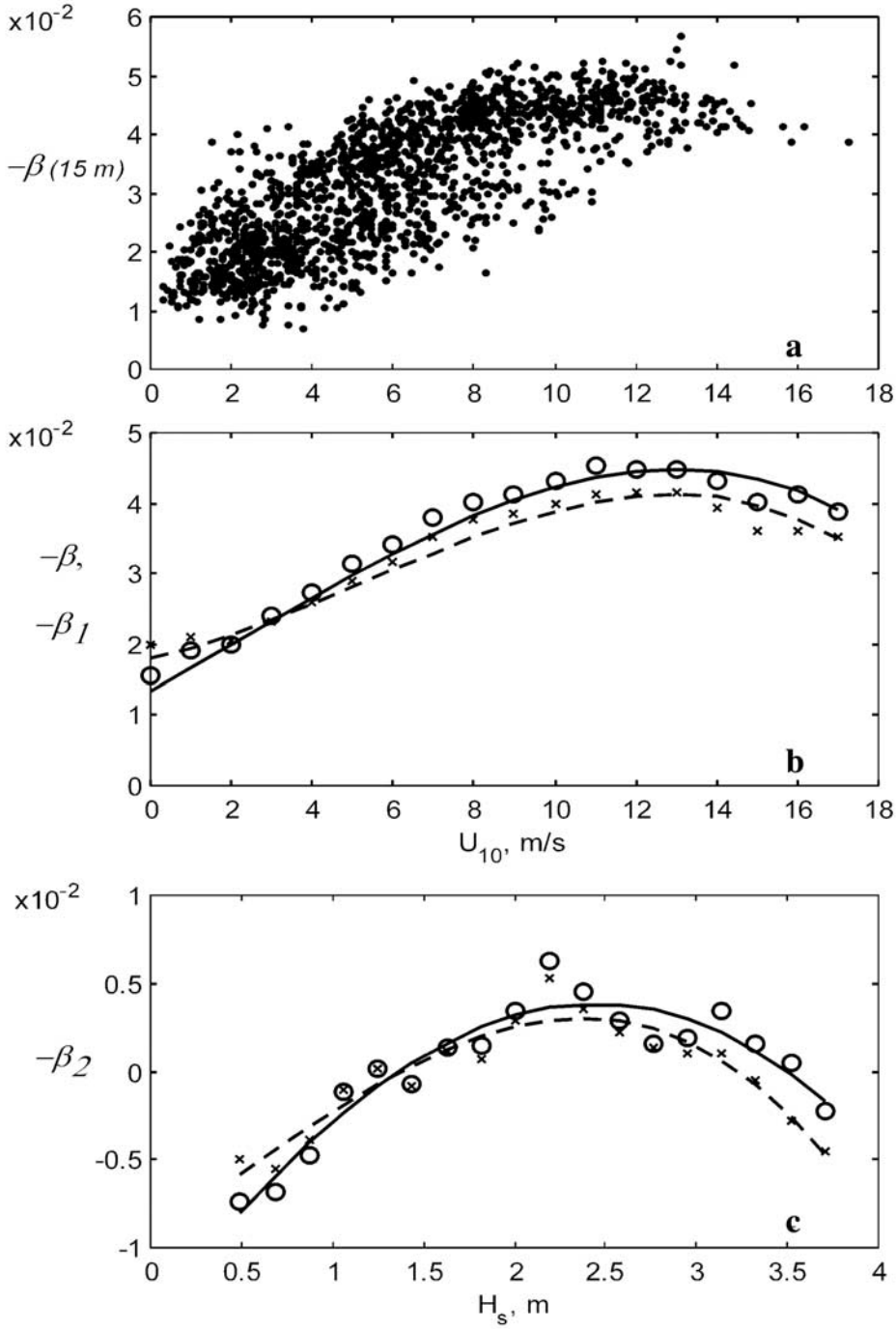

Figure 6. Averages (1 hour) and binned normalized EM bias data $\beta = \epsilon/H_s$, with third-order polynomial fits to U_{10} and H_s. (a) Scatterplot of hourly averaged data for both K15 and K25. (b) $-\beta$ and $-\beta_1(U_{10})$, the polynomial fit to U_{10} as percentages: K15 (circles and solid line) and K25 (crosses and dashed line). (c) $-\beta_2(H_s)$, the polynomial fit to H_s of the residual where $\beta_2 = \beta - \beta_1$. K15 and K25 are as in Figure 6b. Note the nonzero intercepts in both figures.

where, for example, in the (s_l, U_{10}/c) space,

$$x = \alpha(s - s_i) + \left(1 - \alpha^2\right)^{1/2}\left(\frac{U_{10}}{c} - \frac{U_{10}}{c_i}\right) \tag{21}$$

$$y = -\left(1 - \alpha^2\right)^{1/2}(s - s_i) + \alpha\left(\frac{U_{10}}{c} - \frac{U_{10}}{c_i}\right), \tag{22}$$

where e is the relative error, δ is the Dirac delta function, α defines the orientation of the principal axes in the plane, and L_x and L_y are decorrelation length scales in the x and y directions, respectively.

[42] Figures 7e–7h show the results of using the objective mapping to estimate the normalized bias in the (H_s, U_{10}) plane. Overall, we find that the objective mapping only leads to a marginal improvement in the

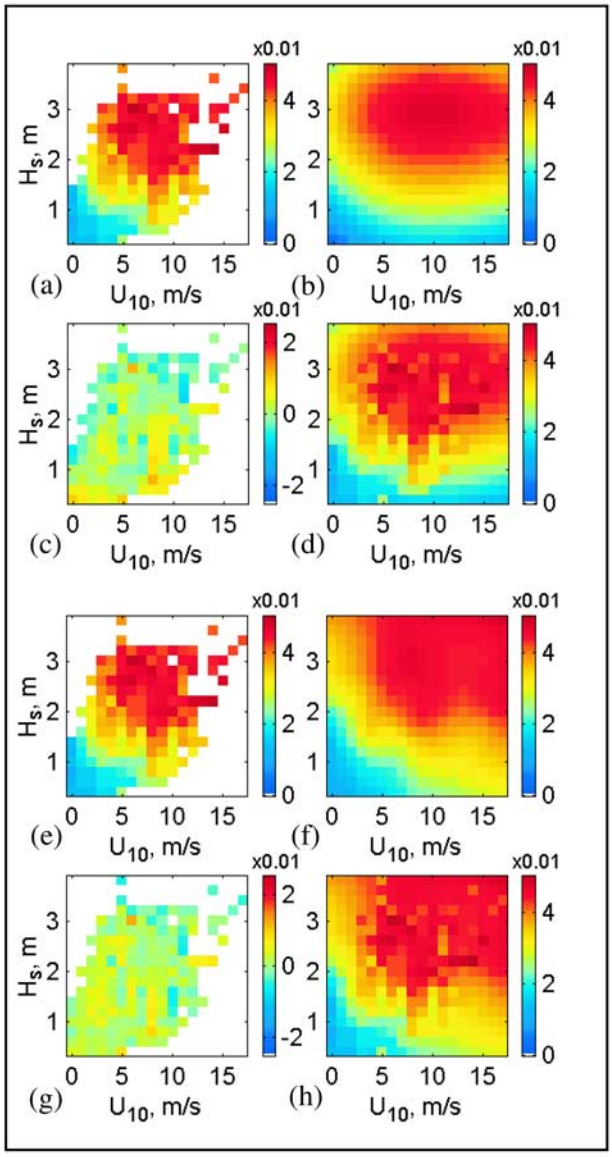

Figure 7. EM bias data with polynomial and optimal estimates (objective mapping) in the (U_{10},H_s) plane. Third-order polynomial fit of (a) the data, (b) the polynomial fit, (c) the error map, and (d) the data merged with the polynomial fit. (e–h) Objective mapping of the data. Figures 7e–7h correspond to Figures 7a–7d. Note the qualitative differences in the estimates of Figures 7b and 7f when the different methods are applied. However, the standard errors for the two methods are essentially the same. See Table 1.

standard error from 0.0062 to 0.0060, when compared with the polynomial fit to the data (Figure 7a).

[43] Figures 9e–9h show the corresponding results for the data in the (s_l, (U_{10}/c)) plane. Here there is no improvement in the standard error, both being 0.0030.

[44] While the use of objective mapping makes no discernable improvement in the standard error of the bias estimation, the error data tabulated in Table 1, clearly shows that the use of wave slope and wave age rather than wave height and wind speed leads to a significant reduction of the error by 52 ± 2% to 0.003 ± 0.0001. See Table 1.

5. Discussion

[45] While dimensional analysis provides support for the relationship $\beta = \beta(a_l k_l, U_{10}/c_l,.)$, it does not give the functional form of the relationship nor illuminate the physical processes. That requires a theory or model. It is clear from Figure 8b that β is proportional to the rms wave slope of the longer waves s_l for $s_l \ll 1$, and essentially independent of the scatterometer elevation in the experiment, giving

$$\beta \approx -0.45 s_l. \tag{23}$$

[46] A variety of processes related to surface waves and electromagnetic scattering by the ocean surface can be represented by an expansion in terms of the surface wave slope and other dimensionless variables including wave age and the normalized bandwidth of the surface wave spectrum. The principal processes that have been considered in accounting for the modulation of the scattering that leads to the EM bias have been short wave (scatterer) modulation and tilt modulation by the longer waves [*Arnold et al.*, 1990; *Arnold*, 1992; *Rodriguez et al.*, 1992; *Elfouhaily et al.*, 2000], both of which can be represented by expansions in terms of the long wave slope. Using a scattering model, *Rodriguez et al.* [1992] concluded that both effects could be equally important, with the altimeter frequency dependence being primarily due to the tilt modulation. *Elfouhaily et al.* [2000] recently concluded that the short wave effects were not accurately represented by earlier theories [*Srokosz*, 1986] but required inclusion of the slope variance ratios that depend on the modulation between short and long waves.

[47] The data presented here show that the wave age effects are secondary to those of wave slope, suggesting that wind forcing (measured by wave age) is a secondary effect also. In the absence of wind forcing, short waves riding on longer waves have their wavelengths shortened (lengthened) and amplitudes increased (decreased) at the crest (trough) of the longer waves [*Longuet-Higgins and Stewart*, 1960]. To leading order, the degree of modulation of the short wave (in amplitude and wave number) is proportional to the wave slope of the longer wave. Equation (23) suggests that β is proportional to the wave slope, qualitatively consistent with the degree of short wave modulation.

[48] This result can be better understood by representing the surface wave distribution using a simple two-scale model. Consider a simple case where the sea surface consists of two waves, a long wave of length much larger than the diameter of the illuminated area of the scatterometer L, and a short wave of wavelength smaller than L. The amplitude, wavelength and wave number of the long wave are a_l, λ_l and k_l, respectively. The reference values of the amplitude, wavelength and wave number of the short wave are a_0, λ_0 and k_0. In addition, we assume that $a_l \gg a_0$. Hence to leading order, the sea surface elevation at a given location along the x axis is

$$\eta = a_l \cos(k_l x). \tag{24}$$

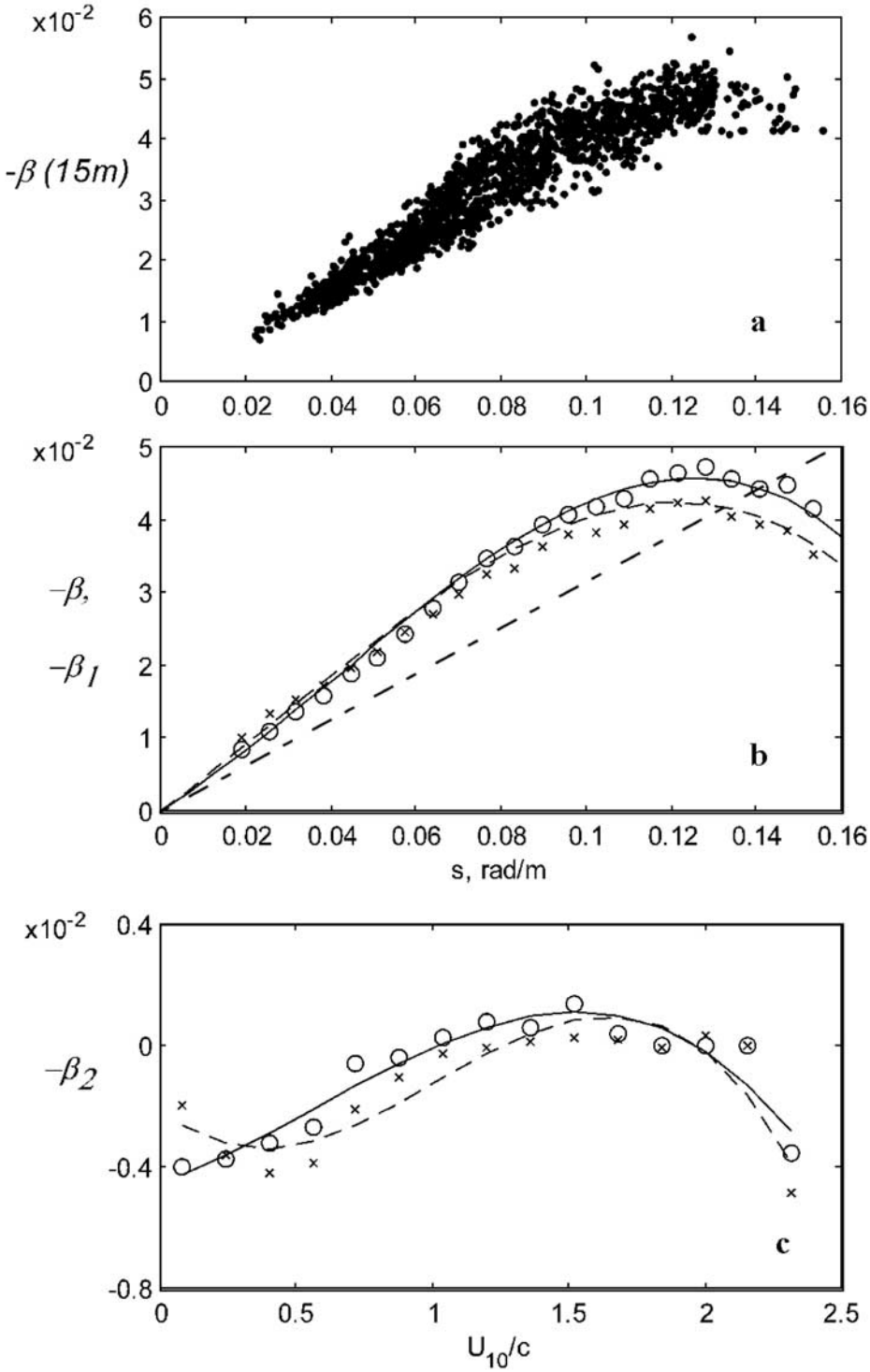

Figure 8. Averages (1 hour) and binned normalized EM bias data $\beta = \epsilon/H_s$, with third-order polynomial fits to s and U_{10}/c. (a) Scatterplot of hourly averaged data for both K15 and K25. (b) $-\beta$ and $-\beta_1(s)$, the polynomial fit to s: K15 (circles and solid line) and K25 (crosses and dashed line). The dashed straight line corresponds to the semiempirical prediction of *Arnold* [1992]. (c) $-\beta_2(U_{10}/c)$, the polynomial fit to U_{10}/c of the residual where $\beta_2 = \beta - \beta_1$. K15 and K25 are as in Figure 8b. Note that the intercept for $\beta_1(s)$ is essentially zero, and the residual in β_2 is now within the range ±0.5% over the whole range of the experiment.

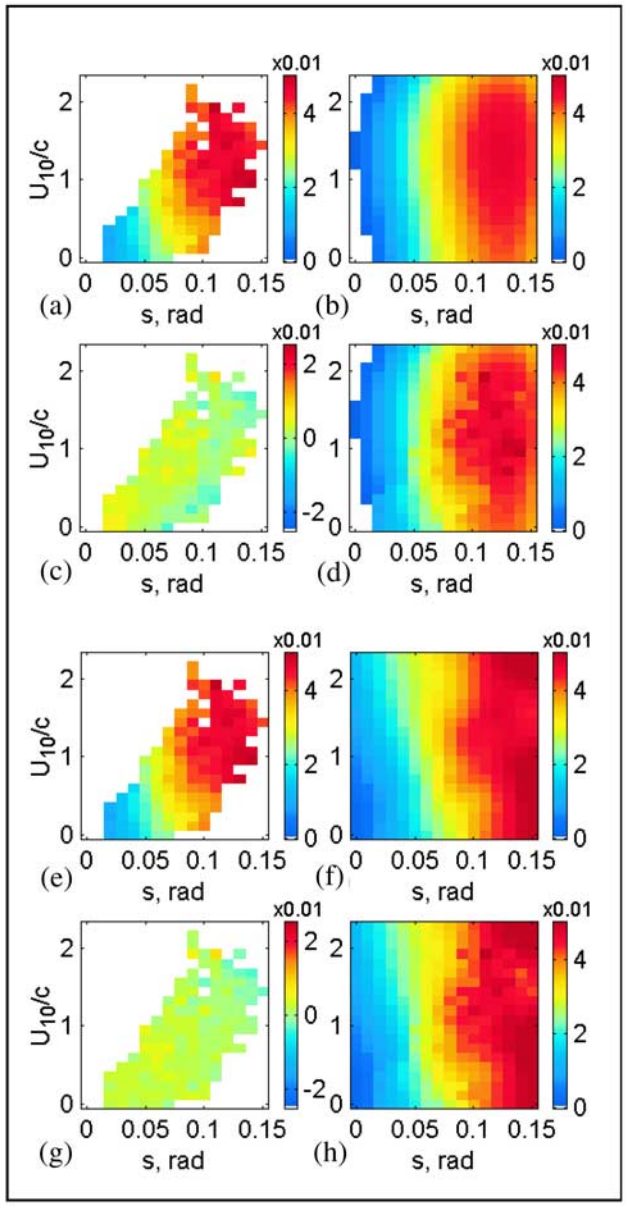

Figure 9. EM bias data with polynomial estimates and objective mapping in the $(s,U_{10}/c)$ plane. Third-order polynomial fit of (a) the data, (b) the polynomial fit, (c) the error map, and (d) the data merged with the polynomial fit. (e–h) Objective mapping of the data, with Figures 9e–9h corresponding to Figures 9a–9d. Note that in this plane the bias is strongly dependent on s but only weakly dependent on U_{10}/c. The standard errors for both estimators in this case are reduced by ~50% when compared with those using U_{10} and H_s.

[49] In the presence of the long wave the amplitude of the short wave, a_s, varies like

$$\frac{a_s}{a_0} = 1 + a_l k_l \cos(k_l x) + O(a_l k_l)^2 \tag{25}$$

or

$$\frac{a_s}{a_0} = 1 + a_l k_l \eta / a_l = 1 + \sqrt{2} s_l \eta / a_l, \tag{26}$$

where s_l is the rms slope of the long waves. Thus the modulation of the short wave amplitude is proportional to the rms long wave slope and the normalized displacement of the short wave from the mean sea level by the long wave.

[50] Perhaps the most convincing case for the role of the modulation of the short waves by the longer waves in explaining the EM bias has been made by the experiments and modeling of *Arnold et al.* [1990, 1995; see also *Arnold*, 1992]. Short wave modulation by longer waves was directly measured and used as input to a physical optics scattering model that gave good agreement with direct measurements of EM bias at Ku and C bands. *Arnold* [1992] examined a similar two-scale (spectral) model relating β to η with a modulation parameter m defined by

$$\frac{a_s}{a_0} = 1 + \sqrt{2} m \eta / a_l. \tag{27}$$

[51] Using wire wave gauge measurements and equation (27) to compute m, and scatterometer measurements from a platform in the Gulf of Mexico, he concluded that

$$\beta = 0.25 \alpha m, \tag{28}$$

where α is a nondimensional parameter whose value depends on the slope and directional characteristics of the short wave spectrum. He suggested that the value of α is in the range $[-1.39, -1.15]$.

[52] Equations (26) and (27) show that, for the simplest two-scale wave field, *Arnold*'s [1992] modulation parameter m is just the rms long wave slope, s_l. Combining this with equation (28) gives

$$\beta = 0.25 \alpha s_l = -(0.32 \pm 0.06) s_l, \tag{29}$$

which is shown with data from this experiment in Figure 7a. When *Arnold*'s [1992] modulation parameter is identified with the rms slope of the longer waves, his two-scale model correctly predicts proportionality between β and s for small wave slopes, while the coefficient in his model is in the range of 64–77% of the empirical value in these experiments.

[53] In a recent model of EM bias, *Elfouhaily et al.* [2001] have stressed the separate importance of long-wave slope and orbital velocity fields in the hydrodynamic modulation of the short waves or scatterers. However, the now classical theories of long wave-short wave interaction [*Longuet-Higgins and Stewart*, 1960; see also *Phillips*, 1981] show that for $c_l/c_s \gg 1$, the leading order effects of short-wave modulation are linear in the long-wave slope. The data from these experiments show that the dominant effect on the normalized bias, β, is due to the long wave slope, with only a weak dependence on wave age. An

Table 1. Standard Errors in β From Polynomial Approximations and Objective Mapping

β	Fitting	(H_s, U_{10})	$(s_l, U_{10}/c)$
β_{15}	third-order polynomial	0.0062	0.0030
β_{25}	third-order polynomial	0.0055	0.0031
β_{15}	objective mapping	0.0060	0.0030
β_{25}	objective mapping	0.0053	0.0029

anonymous referee suggested that the largest values (of the small) residual EM bias occurring at small wave ages (see Figure 8) could be evidence of contamination by swell; however, comparable values of the residual EM bias occur at the largest wave ages! Furthermore, as mentioned above, a preliminary study of the coherence between the backscattered power and the surface wave spectrum shows that the contribution to the EM bias is predominantly from the longer waves that contribute most to the slope. This would appear to exclude any significant influence of the swell. However, a conclusive study of the influence of swell would require good directional wave measurements, that can separate wind seas and swell by both their directional properties and their frequencies.

[54] Our use of a constant Charnock parameter in equation (5), which neglects recent observations of the dependence of the parameter on wave age [e.g., *Drennan et al.*, 2003] and other variables may influence the values of U_{10} used here. The measurement and characterization of the drag coefficient over the ocean (equivalent to measuring z_0) is an important area of current research which goes well beyond the limits of this study. However, in this case its importance is mitigated by the secondary role of the residual EM bias which is not accounted for by the wave slope and is correlated here with the wave age which depends on U_{10}. Nevertheless, it points to the need for further direct measurements of EM bias with state-of-the-art atmospheric boundary layer measurements in which u_* is directly measured and the applicability of Monin-Obukhov scaling of the atmospheric boundary layer is tested.

[55] Together the use of wave slope and wave age rather than wind speed and wave height leads to a reduction by $\sim$50% in the error of the EM bias estimates. These improvements are independent of whether we use polynomial fits or objective mapping of the data. We believe that these reductions in the errors are sufficient to justify an examination of how information on wave slope and wave age can be included in operational algorithms for EM bias. *Glazman and Srokosz* [1991] have suggested that ''pseudo'' wave parameters (especially wave age) might be inferred from the classical fetch relationships for wind waves, but there are good reasons why this approach would not work in altimetry. One of the principal uses of radar altimetry is in using the measured sea surface slope to infer the geostrophic currents, the classical examples being across western boundary currents over which the sea surface height may vary by O(1) m. However, wave-current interaction can significantly modify the slope of the surface waves, especially in current gradients, and, according to the measurements presented here, modify the EM bias. Thus the bias is correlated with the desired measurement in a way that cannot be resolved unless the slope is directly measured, or inferred from a model that accounts for these effects. We believe that efforts to globally measure and model the surface wave field in support of radar altimetry will lead to significantly improved algorithms for EM bias.

[56] The beginnings of this approach are explored in a very recent paper by *Kumar et al.* [2003]. They considered the use of operational wave model (WAM) data and buoy measurements of the wind and wave field to implement a version of the empirical wave-slope/wave-age algorithm based on the data from this work, finding good agreement with the theoretical EM bias model of *Srokosz* [1986] over a range of parameters. However, more work is needed to extend the range of wave slopes. They found a significant correlation between high-frequency sea surface height fluctuations and operational EM bias corrections based on satellite data and variance minimization techniques [*Gaspar et al.*, 1994]. This implies that improved operational EM bias algorithms cannot be based on altimeter data alone, and may require input from wind wave and coupled ocean-atmosphere models and perhaps other satellite sensors.

[57] Following this semiempirical investigation of the role of the sea surface slope in the representation of the EM bias, which has shown the correspondence between the wave slope and the modulation parameter in the two-scale physical optics model, K. F. Warnick et al. (Theoretical model of electromagnetic bias based on RMS wave slope, submitted to *Journal of Geophysical Research*, 2002) have developed a slightly improved version of the two-scale model proposed by *Arnold et al.* [1991] and *Arnold* [1992], which gives very good agreement with the Ku band measurements of *Arnold et al.* [1995] from the Gulf of Mexico. The agreement to within 10% of the best linear fit to the Gulf of Mexico data contrasts with the 23–36% difference with this data from Bass Strait. These differences between the data sets, which were obtained with the same equipment and techniques, remain unresolved.

[58] It is still the case that a complete data set over a wide range of environmental conditions, including direct measurements of EM bias, the directional spectrum of the surface wave field, sea surface height and surface currents and winds, which would permit a thorough investigation of EM bias for operational altimetry, does not exist. In view of the critical role of altimetry in global oceanography, air-sea interaction and climate sciences, it is imperative that errors in estimating EM bias be improved to avoid misinterpreting unresolved bias errors as seasonal, interannual or secular signals in sea surface height and currents.

[59] **Acknowledgments.** This experiment would not have been possible without the generosity of Esso/BHP in permitting us to use the platform and without the efforts of the superintendent and crew of the Snapper Platform in monitoring the data acquisition for a 3 month period. We thank Ian Jones of Sydney University for facilitating these efforts and Lawson and Treloar (Australia) for supplying meteorological data from the Kingfish B platform. We thank Ron Horn for software development and installation, Eric Terrill for logistical support of the experiment, and Anatol Rozenberg for preparation and calibration of the scatterometers. We thank two anonymous referees of the original paper for their helpful comments and questions. This work was supported by a grant to W.K.M. from NASA and by a subcontract from Brigham Young University.

References

Arnold, D. V. (1992), Electromagnetic bias in radar altimetry at microwave frequencies, Ph.D. thesis, Mass. Inst. of Technol., Cambridge.

Arnold, D. V., W. K. Melville, and J. A. Kong (1990), Theoretical prediction of EM bias, in *Oceans 90 Proceedings: Engineering in the Ocean Environment*, pp. 253–256, IEEE Press, Piscataway, N. J.

Arnold, D. V., J. A. Kong, and W. K. Melville (1991), Physical optics prediction of EM bias, in *Proceedings, Progress in Electromagnetic Research*, 169 pp., IEEE Press, Piscataway, N. J.

Arnold, D. V., W. K. Melville, R. H. Stewart, J. A. Kong, W. C. Keller, and E. Lamarre (1995), Measurements of electromagnetic bias at Ku and C bands, *J. Geophys. Res.*, *100*, 969–980.

Casella, G. (1990), *Statistical Inference*, 650 pp., Brooks/Cole, Pacific Grove, Calif.

Chelton, D. B. (1994), The sea state bias in altimeter estimates of sea level from collinear analysis of TOPEX data, *J. Geophys. Res.*, *99*, 24,995–25,008.

Cox, C. S., and W. H. Munk (1956), Slopes of the sea surface deduced from photographs of sun glitter, *Bull. Scripps Inst.*, *6*, 401–488.
Daley, R. (1991), *Atmospheric Data Analysis*, 457 pp., Cambridge Univ. Press, New York.
Doviak, R. J., and D. S. Zrnic (1984), *Doppler Radar and Weather Observations*, 458 pp., Academic, San Diego, Calif.
Drennan, W. M., H. C. Graber, D. Hauser, and C. Quentin (2003), On the wave age dependence of wind stress over pure wind seas, *J. Geophys. Res.*, *108*(C3), 8062, doi:10.1029/2000JC000715.
Elfouhaily, T., D. R. Thompson, B. Chapron, and D. Vandemark (2000), Improved electromagnetic bias theory, *J. Geophys. Res.*, *105*, 1299–1310.
Elfouhaily, T., D. R. Thompson, B. Chapron, and D. Vandemark (2001), Improved electromagnetic bias theory: Inclusion of hydrodynamic modulations, *J. Geophys. Res.*, *106*, 4655–4664.
Fedorov, A. V., W. K. Melville, and A. Rozenberg (1998), An experimental and numerical study of parasitic capillary waves, *Phys. Fluids*, *10*, 1315–1323.
Felizardo, F. C., and W. K. Melville (1995), Correlations between ambient noise and the ocean surface wave field, *J. Phys. Oceanogr.*, *25*, 513–532.
Gaspar, P., and J.-P. Florens (1998), Estimation of the sea state bias in radar altimeter measurements of sea level: Results from a new nonparametric method, *J. Geophys. Res.*, *103*, 15,803–15,814.
Gaspar, P., F. Ogor, P.-Y. Le Traon, and O.-Z. Zanifé (1994), Estimating the sea state bias of the TOPEX and Poseidon altimeters from crossover differences, *J. Geophys. Res.*, *99*, 24,981–24,994.
Glazman, R., and M. Srokosz (1991), Equilibrium wave spectrum and sea state bias in altimetry, *J. Phys. Oceanogr.*, *21*, 1609–1621.
Gommenginger, C. P., M. A. Srokosz, J. Wolf, and P. A. E. M. Janssen (2003), An investigation of altimeter sea state bias theories, *J. Geophys. Res.*, *108*(C1), 3011, doi:10.1029/2001JC001174.
Hevizi, L. G., E. J. Walsh, R. E. McIntosh, D. Vandemark, D. E. Hines, R. N. Swift, and J. F. Scott (1993), Electromagnetic bias in sea surface range measurements at frequencies of the TOPEX/Poseidon satellite, *IEEE Trans. Geosci. Remote Sens.*, *31*, 367–388.
Jessup, A. T. (1990), Detection and characterization of deep-water wave breaking using moderate incidence angle microwave backscatter from the sea surface, Ph.D. thesis, Mass. Inst. of Technol.-Woods Hole Oceanogr. Inst. Joint Prog., Cambridge, Mass.
Jessup, A. T., W. K. Melville, and W. C. Keller (1991), Breaking waves affecting microwave backscatter: 1. Detection and verification, *J. Geophys. Res.*, *96*, 20,547–20,559.
Komen, G. J., L. Cavaleri, M. Donelan, K. Hasselmann, S. Hasselman, and P. A. E. M. Janssen (1994), *Dynamics and Modelling of Ocean Waves*, 532 pp., Cambridge Univ. Press, New York.
Kumar, R., D. Stammer, W. K. Melville, and P. Janssen (2003), Electromagnetic bias estimates based on TOPEX, buoy, and wave model data, *J. Geophys. Res.*, *108*(C11), 3351, doi:10.1029/2002JC001525.
Large, W. G., and S. Pond (1981), Open ocean momentum flux measurements in moderate to strong winds, *J. Phys. Oceanogr.*, *11*, 324–336.
Longuet-Higgins, M. S., and R. W. Stewart (1960), Changes in the form of short gravity waves on long waves and tidal currents, *J. Fluid Mech.*, *8*, 565–583.
Melville, W. K., R. H. Stewart, W. C. Keller, J. A. Kong, D. V. Arnold, A. T. Jessup, M. R. Loewen, and A. M. Slinn (1991), Measurements of electromagnetic bias in radar altimetry, *J. Geophys. Res.*, *96*, 4915–4924.
Melville, W. K., F. C. Felizardo, and P. Matusov (1999), Measurements of sea-state bias, poster presented at the Air-Sea Interface Symposium, Sydney, 11–15 Jan.
Millet, F. W., D. V. Arnold, K. F. Warnick, and J. Smith (2003a), Electromagnetic bias estimation using in situ and satellite data: 1. RMS wave slope, *J. Geophys. Res.*, *108*(C2), 3040, doi:10.1029/2001JC001095.
Millet, F. W., D. V. Arnold, P. Gaspar, K. F. Warnick, and J. Smith (2003b), Electromagnetic bias estimation using in situ and satellite data: 2. A nonparametric approach, *J. Geophys. Res.*, *108*(C2), 3041, doi:10.1029/2001JC001144.
Phillips, O. M. (1981), The dispersion of short wavelets in the presence of a dominant long wave, *J. Fluid Mech.*, *107*, 465–485.
Rodriguez, E., Y. Kim, and J. M. Martin (1992), The effect of small-wave modulation on the electromagnetic bias, *J. Geophys. Res.*, *97*, 2379–2389.
Smith, S. D. (1988), Coefficients for sea surface wind stress, heat flux, and wind profiles as a function of wind speed and temperature, *J. Geophys. Res.*, *93*, 15,467–15,472.
Srokosz, M. (1986), On the joint distribution of surface elevation and slopes for a nonlinear random sea, with an application to radar altimetry, *J. Geophys. Res.*, *91*, 995–1006.
Walsh, E. J., et al. (1991), Frequency dependence of electromagnetic bias in radar altimeter sea surface range measurements, *J. Geophys. Res.*, *96*, 20,571–20,583.
Wu, J. (1980), Wind stress coefficients over the sea surface near neutral conditions—A revisit, *J. Phys. Oceanogr.*, *10*, 727–740.
Yaplee, B., A. Shapiro, D. Hammond, B. Au, and E. Uliana (1971), Nanosecond radar observations of the ocean surface from a stable platform, *IEEE Trans. Geosci. Electron.*, *9*, 170–174.

F. C. Felizardo, Union Cement Corporation, 39 Plaza Drive, Rockwell Center, Makati City, Philippines. (fcf.ucc@phinma.com.ph)
W. K. Melville and P. Matusov, Scripps Institution of Oceanography, University of California, San Diego, La Jolla, California, 92093-0213, USA. (kmelville@ucsd.edu; pmatusov@ucsd.edu)